Atmos. Chem. Phys. Discuss., 14, 7711–7737, 2014
www.atmos-chem-phys-discuss.net/14/7711/2014/
doi:10.5194/acpd-14-7711-2014

Atmospheric Chemistry and Physics Discussions

Countergradient heat flux observations during the evening transition period

E. Blay-Carreras[1], E. R. Pardyjak[2], D. Pino[1,3], D. C. Alexander[2], F. Lohou[4], and M. Lothon[4]

[1]Department of Applied Physics, Universitat Politècnica de Catalunya – BarcelonaTech, Barcelona, Spain
[2]Department of Mechanical Engineering, University of Utah, Salt Lake City, UT, USA
[3]Institute of Space Studies of Catalonia (IEEC–UPC), Barcelona, Spain
[4]Université de Toulouse/CNRS 5560, Laboratoire d'Aérologie, Toulouse, France

Received: 4 March 2014 – Accepted: 4 March 2014 – Published: 21 March 2014

Correspondence to: E. Blay-Carreras (estel.blay@upc.edu)

Published by Copernicus Publications on behalf of the European Geosciences Union.

Abstract

Gradient-based turbulence models generally assume that the buoyancy flux ceases to introduce heat into the surface layer of the atmospheric boundary layer in temporal consonance with the gradient of the local virtual potential temperature. Here, we hypothesize that during the evening transition a delay exists between the instant when the buoyancy flux goes to zero and the time when the local gradient of the virtual potential temperature indicates a sign change. This phenomenon is studied using a range of data collected over several Intensive Observational Periods (IOPs) during the Boundary Layer Late Afternoon and Sunset Turbulence field campaign conducted in Lannemezan, France. The focus is mainly on the lower part of the surface layer using a tower instrumented with high-speed temperature and velocity sensors.

The results from this work confirm and quantify a flux-gradient delay. Specifically, the observed values of the delay are ~30–80 min. The existence of the delay and its duration can be explained by considering the convective time scale and the competition of forces associated with the classical Rayleigh–Bénard problem. This combined theory predicts that the last eddy formed while the sensible heat flux changes sign during the evening transition should produce a delay. It appears that this last eddy is decelerated through the action of turbulent momentum and thermal diffusivities, and that the delay is related to the convective turn – over time – scale. Observations indicate that as horizontal shear becomes more important, the delay time apparently increases to values greater than the convective turnover time-scale.

1 Introduction

The general behavior of the diurnal cycle of the atmospheric boundary layer (ABL) under clear sky fair weather conditions is well-known (Stull, 1988). During the day, a convective boundary layer driven by surface and entrainment fluxes exists (Moeng and Sullivan, 1994; Sorbjan, 1996; Sullivan et al., 1998; Pino et al., 2003; Fedorovich

ACPD
14, 7711–7737, 2014

et al., 2001). Late in the afternoon, due to radiative cooling of the ground, a stable boundary layer (SBL), where turbulence may be suppressed, is created adjacent to the earth's surface (Nieuwstadt, 1984; Mahrt, 1998; Beare et al., 2006). A residual layer (RL) of weak turbulence exists above this SBL. The RL occupies a similar space as the mixed layer of that day's convective boundary layer (CBL). However, the details of certain processes, particularly those associated with non-stationary transitional periods are not as well understood. The transition occurring after the peak in solar insulation can be divided into to distinct periods: the *afternoon transition*, when the surface sensible heat flux starts to decrease from its midday maximum, and the *evening transition*, when the surface sensible heat flux becomes negative (Nadeau et al., 2011).

This paper focuses on the behavior of the buoyancy flux and temperature gradient in the surface layer during the early and late evening transition period by analyzing measurements obtained during the Boundary Layer Late Afternoon and Sunset Turbulence (BLLAST, Lothon et al., 2012; Lothon and Lenschow, 2010) field campaign. BLLAST was conceived to study the late afternoon transition (LAT) processes in the ABL. Objectives of the BLLAST project include gaining a better understanding of (a) the importance of surface heterogeneity on the LAT and (b) the structure and evolution of the boundary layer itself during this period of the day. The team members of this project include an international group of scientists from different countries in Europe and the USA. The main hypotheses to be tested during this study are focused on the afternoon transition; therefore, the observations obtained from BLLAST campaign provide a valuable framework to develop the present work.

The hypothesis of this work is that during the evening transition, a delay exists between the instant when the buoyancy flux goes to zero and the time when the local gradient of the virtual potential temperature indicates a sign change. Ghan (1981) and Franchitto and Rao (2003) attempted to find a relationship between the temperature gradient and the heat flux, considering the complete cycle. Moreover, non-local model studies were used to develop different theories about the eddy diffusivity and countergradient transport, which can affect this relation (Deardorff, 1972; Holtslag

ACPD
14, 7711–7737, 2014

and Moeng, 1991). Nonetheless, it is normally assumed that the buoyancy flux ceases to introduce heat into the ABL at the same instant that the gradient of the virtual potential temperature reflects this phenomenon. Most simulation models work using this basic concept. A good knowledge of the phenomenon and evolution of the afternoon/evening transition is crucial for developing more realistic models and creating better approximations (Sorbjan, 1997; Cole and Fernando, 1998; Edwards et al., 2006; Pino et al., 2006; Angevine, 2007; Nadeau et al., 2011).

Some investigations (Grimsdell and Angevine, 2002; Pino et al., 2006), reflect a continuation of heating after the sensible heat flux becomes negative from the upper part of the atmosphere via entrainment process. However, no other in depth studies focusing on the reaction of the surface layer during this transition has ever been reported. The objective of this article is to investigate this phenomenon using a range of data collected over several days, focusing mainly on the lower surface layer, using a tower instrumented with fast response fine-wire (FW) thermocouples and sonic anemometers thermometers (SATs). Moreover, the hypothesis will be supported by theories that can explain this phenomenon, such as the inverse Bénard problem, the effect of convective time or the definition of convection characteristics with the help of the Monin–Obukhov length scale.

The paper is structured as follows. In Sect. 2, we present the theory supporting the main hypothesis of the article. In Sect. 3, we describe the BLLAST field campaign and the instruments selected to test the hypothesis including the method for identifying time periods of interest for the analysis. In Sect. 4, we present the results focusing on the delay and convective time analysis, the Monin–Obukhov length scale analysis and turbulent Rayleigh number analysis. Finally, Sect. 5 summarizes the results.

2 Background theory

The hypothesis, which was described in the introduction, can be related to the well-known Rayleigh–Bénard (R–B) problem (thermal instability) associated with the

ACPD
14, 7711–7737, 2014

heating of a quiescent layer of fluid from below which ultimately results in turbulent free convection (Kundu, 2010). The standard R–B problem is based on the idea that there is a layer of fluid heated from below, however, the upper part of the layer is heavy enough to stifle the convective movements. Both viscosity and thermal diffusivity make it difficult for convection movements to happen. Therefore, large temperature gradients are required to create the instability that makes movement possible. Here we consider similar physics, but in the opposite sense because during LAT the CBL is cooled from below. The idea was previously introduced and experimentally studied by Cole and Fernando (1998) who designed a laboratory water tank experiment to observe the decay of temperature and velocity fluctuations in the CBL in response to cooling the surface.

In both the classical R–B problem and the phenomena studied in this paper, a delay exists that is related with the buoyancy flux at the surface and convective movements. When the buoyancy flux ceases, the convective movements continue for some time. This delay can be similarly produced from the same factors that drive the classical R–B problem. In other words, the viscosity and the thermal diffusivity make it possible for this transition to happen in a more smooth way. The dimensionless parameter, which compares the destabilizing forces (buoyancy forces) with the stabilizing forces (viscosity and thermal diffusivity) is the Rayleigh number,

$$Ra = \frac{g\Delta\overline{\theta_v}(\Delta z)^3}{\overline{\theta_v}\kappa\nu}, \quad (1)$$

where g is the gravitational constant, $\Delta\overline{\theta_v}$ is the average virtual potential temperature difference over the layer depth Δz (taken here as the height of the atmospheric near–surface layer), κ is the molecular thermal diffusivity and ν is the molecular kinematic viscosity. For the classical R–B problem with heating from below, when the Rayleigh number reaches a critical value, Ra_{cr}, convective movement will start. In this paper, we provide preliminary evidence for a transitional turbulent Rayleigh number at which convective motions cease.

ACPD
14, 7711–7737, 2014

3 Methodology

This study was performed within the framework of the BLLAST field campaign. Amongst the wide range of instruments deployed during the campaign, a relatively short (10 m), but highly instrumented tower was selected to be used in this study. This tower, located at 43°07′39.3″ N and 0°21′57.9″ E, was selected because it was equipped with a large number of closely spaced sensors, and was placed over relatively simple and homogeneous terrain (flat grass field). The sensors deployed on the tower included SATs and FWs. The instrument–deployment strategy focused many sensors close to the ground in order to observe small and fast changes connected to this zone. Figure 1a shows the vertical location of the instruments on the 10 m mast and Fig. 1b shows an aerial view of the site where the tower was located.

Four Campbell Scientific sonic anemometer thermometers (CSAT3, Logan, UT) fit with 12.7 µm diameter Campbell Scientific E-TYPE model FW05 fine-wire thermocouples were mounted at the following heights: 2.23, 3.23, 5.27 and 8.22 m above ground. Closer to the ground, there were four additional FW05 sensors mounted at 0.091, 0.131, 0.191, and 0.569 m above ground. The lowest sensor was placed just in the grass canopy. The grass around this sensor was regularly trimmed to maintain a canopy height of approximately 7–9 cm. Sensors collected data from 1 June to 6 July 2011. During the intensive observation periods (IOPs) the lowest FWs were installed during the afternoon through the entire transition period to provide an expanded dataset. All instruments recorded date at 20 Hz. However, 5 min block-averaged data are presented in the analysis shown below. All data were processed using the software package *EC-pack* (Van Dijk et al., 1998).

This study focuses on the analysis of the following group of IOP days during the BLLAST campaign: 24, 25, 27, 30 June and 1, 2 July 2011 when the 10 m tower was completely instrumented. Table 1 summarizes the information used to characterize the IOPs including the daily maximum surface sensible heat flux, the duration of the diurnal cycle and the days from the last rainfall.

ACPD
14, 7711–7737, 2014

The primary goal of this work is to characterize and understand the observed time delay between the instant when the buoyancy flux is zero and when the virtual potential temperature gradient changes sign. To sketch the change of sign of the gradient of virtual potential temperature, Fig. 2 shows the temporal evolution of the vertical profile of potential temperature measured by the FWs located at the 10 m mast during the evening on 1 July 2011. We can observe how, at the lowest levels, the gradient of potential temperature changes sign from negative to positive.

The instrumentation used in the campaign included fewer SATs than FW thermocouples, so the instruments were not always collocated. However, to include the effects of humidity, we use the measurements made by the SATs located at 2.23 and 3.23 m because these are the lowest sensors which can be used to simultaneously measure virtual potential temperature gradients and buoyancy flux.

To estimate the virtual potential temperature (θ_v), we assumed that the virtual temperature (T_v) can be approximated by the sonic temperature. The virtual potential temperature was then estimated using the adiabatic lapse rate (Γ) as follows: $\theta_v = T_v + \Gamma z$. Gradients were then computed using finite differences (Chapra and Canale, 1998).

The following paragraphs describe how this delay is determined. Figure 3 shows the observed temporal evolution of θ_v at 2.23 and 3.23 m during two IOP and illustrates the time when the change in sign of the gradient between the virtual potential temperature at the two levels occurs. The change in sign of the gradient first occurs at 18:36 UTC for 30 June 2011 and at 18:51 UTC on 1 July 2011. The buoyancy flux was computed using:

$$\mathrm{BF} = \frac{g}{T_v}\overline{w'\theta'_v}. \quad (2)$$

Here, $\overline{w'\theta'_v}$ is the vertical kinematic flux of virtual potential temperature. The lowest sensor (2.23 m) is used to define when the buoyancy flux ceases. In other words, when there is no more heat coming from the ground being measured at that probe. For

ACPD
14, 7711–7737, 2014

instance, on 30 June and on 1 July 2011 the lower sensor shows that the flux ceases at approximately 18:18 and 17:54 UTC, respectively. The delay time between when temperature gradient and buoyancy flux pass through zero is then simply the difference between the two times.

To develop the theory for the inverse R–B problem, the area selected is the lower surface layer specifically from 2.23 to 8.2 m, which is the area with an evolution closer to the idea proposed by Bénard. First, we calculate the turbulent thermal diffusivity (K_H) and the turbulent viscosity (K_M). These two parameters can be estimated using the following equations.

$$K_H = \overline{w'\theta'_v} \Big/ \frac{\partial \overline{\theta_v}}{\partial z}, \tag{3}$$

$$K_M = -u_*^2 \Big/ \frac{\partial S}{\partial z}, \tag{4}$$

where u_* is the friction velocity and S is the mean wind speed. There is relatively little variability in these parameters during the day, therefore they are estimated by using the maximum buoyancy flux to avoid possible influences of the skin flow close to the afternoon transition and to be consistent during all IOPs.

4 Results and discussion

4.1 Delay time analysis

Using the procedure described above, the delay time (DT) was computed for all IOPs. The results for all the studied IOPs are summarized in Fig. 4, where the instants when the buoyancy flux and the virtual potential temperature gradient change sign are shown. As is shown in the figure, this delay was present on all days analyzed. The delay varies from around 30–80 min. The numerical values for the delay time for all IOPs are given in Table 1.

ACPD
14, 7711–7737, 2014

A possible explanation for the occurrence of this delay can be related to eddy movements associated with warm air plumes that form at the surface. The moment that the buoyancy flux transitions from positive to negative values indicates that no more heat is being introduced in the atmosphere from the ground. Additionally, the upward movement due to warming of the air next to the ground (formation of new thermal plumes) also stops. However, these movements are not instantaneous movements. Quite the opposite, these movements start at the ground, mix through the surface layer and potentially move upward through entire boundary layer up to the entrainment zone and then descend with the warm air introduced by the overshoots of the eddies in the free atmosphere (i.e. the movements act over an eddy turnover period of time). When the introduction of heat stops (BF = $0\,\mathrm{W\,m^{-2}}$), the last eddy forms and continues the movement of the boundary layer. During this eddy turnover time period, the surface layer is cooled up through the height at which the temperature gradient is being measured. Consequently, the surface layer does not instantaneously feel when the surface flux halts because the mixing (and transfer of heat) continues through an eddy turnover time. This idea has been presented in different studies, for instance by Sorbjan (1997) or van Driel (2011), although, it is mainly focused on movements in the entrainment zone and not at the ground.

An analysis of the dimensionless temperature gradient (ϕ_h), as described by Monin–Obukhov Similarity Theory (MOST), was used to investigate the presence of this delay. Theoretically, the Monin–Obukhov length scale (L) should include the effects associated with synoptic scale motion (Stull, 1988). L can be used as a scaling parameter to define the convective characteristics of the atmospheric boundary layer. Using this parameter, the effects of buoyancy and mechanical production of turbulence can be compared at a specific altitude. The surface layer scaling parameter ($-z/L$) provides a metric indicating the strength of the convective conditions during the IOP

ACPD
14, 7711–7737, 2014

period leading into the evening transition. We computed ϕ_h and $-z/L$ as follows:

$$\phi_h = \frac{kz}{\theta_{v*}^{SL}} \frac{\partial \theta_v}{\partial z} = \frac{kzu_*}{-\overline{w'\theta'_v}} \frac{\partial \theta_v}{\partial z}, \quad (5)$$

$$-\frac{z}{L} = \frac{kzg\left(\overline{w'\theta'_v}\right)_s}{\overline{\theta_v} u_*^3}. \quad (6)$$

where k is the von Karman constant, z is the analysis altitude (2.23 m).

Figure 5 shows every 5 min ϕ_h as a function of $-z/L$ at 2.23 m for 30 June and 1 July 2011. Clearly, there are points which break away from MOST (indicated by the dashed black line). Specifically, gradient-theory fails locally due to the counter-gradient observations that appear in the plots during near stable conditions. Formally, MOST should be valid in the stable layer. However, during the transition period, one can observe that the log surface layer locally disappears close to the ground as there is a decoupling between the old log-layer and the newly forming stable layer, as shown in the transitioning temperature profile in Fig. 2. In the past, this phenomenon was mainly observed for the air–sea boundary layer (Sahlee, 2008). However, Smedman (2007) also observed this behavior at a site over land, but for atmospheric conditions that were quite different from our study case. In particular, their case was for strong winds between 7 and 10 $m\,s^{-1}$ in contrast with BLLAST calm conditions.

4.2 Convective time analysis

To provide support for our delay hypothesis, the convective time scale is analyzed and compared to the delay time scale. The convective time scale can be defined as the approximate time that it takes one eddy to traverse the atmospheric boundary layer. The hypothesis described above should be supported, if the value of the delay and the value of the convective time are similar. In other words, the delay exists as a result of

ACPD
14, 7711–7737, 2014

the continued movement of the boundary layer due to the last eddy motions generated at the surface.

It should be noted that there is debate in the research community regarding the use of various time scales during the transition period. There is not a general agreement about which scaling time is the best option during afternoon/evening transition (Nieuwstadt and Brost, 1986; Lothon et al., 2012). However, it will be used to learn more about the theory proposed.

First, the convective time scale (t_*) is computed following Deardorff (1972):

$$t_* = \frac{z_i}{w_*}, \quad \text{where} \quad w_* = \left[\frac{g z_i}{\overline{\theta_v}} \overline{w'\theta'_v}\right]^{\frac{1}{3}} \tag{7}$$

being z_i the boundary-layer depth. These scales are then computed using the averaging period just before the buoyancy flux vanishes. The depth of the boundary layer was obtained from the ceilometer installed for the BLLAST campaign very close to the tower used in this analysis. This instrument uses a laser diode at a wavelength of 905 nm to measure the height of cloud bases up to 7600 m (Haeffelin, 2012).

The results from the calculation of the convective time scale for all IOPs are shown in Table 1 and Fig. 6. It is clear that the delay time and the convective time compare better on some IOPs than others. For some IOPs, such as 24 June and 30 June 2011, the delay time is nearly the same as the convective time. However, on other days, such as 25 or 27 June, the convective scale and delay time compare quite poorly.

These observed differences between the time scales could be a result of the characteristics of the boundary layer associated with the different IOPs that are not accounted for in the assumptions associated with the convective time scale. In other words, IOPs associated with very convective conditions seem to follow the theory better, while more synoptically forced conditions fail.

ACPD
14, 7711–7737, 2014

4.3 Monin–Obukhov length analysis

In contrast to Sect. 4.1, here we computed a characteristic surface layer scaling parameter ($-z/L$) for each of the IOPs by averaging it over the time period prior to the main evening transition (from 12:00 to 16:45 UTC). From the results, we observe that each IOP can be classified as a convective or weakly convective day (see Table 1). The most convective IOPs were 24 and 30 June 2011. These IOPs were also those with a better correlation between the delay time and the convective time scale (see Fig. 6 and Table 1). On the other hand, the weaker convective days (i.e., 25 and 27 June 2011) show larger difference between the delay and convective times (see Table 1). Less convective days have higher values of u_* as a result of increased mechanical turbulence production close to the ground (2.23 m). On these weakly convective days, the delay time is increased as shear prevents the rapid onset of a stable boundary layer at the surface.

Figure 7 shows the difference between the two time scales as a function of $-z/L$. Evidently, the BLLAST data indicate an exponentially decreasing relationship between the time scale and the Monin–Obukhov parameter. This relationship is likely to be a function of local effects and should be investigated at other sites to see if a general relationship can be ascertained. Regardless, Fig. 7 shows a potentially site specific method for forecasting the delay time using midday data from a single flux tower.

4.4 Turbulent Rayleigh number analysis

The Turbulent Rayleigh number (Ra_{turb}) can be used to explain the behavior of the delay time. It is calculated with Eq. (1) but instead to use molecular thermal diffusivity (κ) and molecular kinematic viscosity (ν), we use the turbulent thermal diffusivity (see Eq. 3) and turbulent viscosity (see Eq. 4). Therefore, Ra_{turb} reads:

$$Ra_{\mathrm{turb}} = \frac{g}{\overline{\theta_{\mathrm{v}}}} \frac{\Delta\overline{\theta_{\mathrm{v}}}(\Delta z)^3}{K_{\mathrm{H}} K_{\mathrm{M}}} = -\frac{g}{\overline{\theta_{\mathrm{v}}}} \frac{(\Delta\overline{\theta_{\mathrm{v}}})^2 \Delta S \Delta z}{\overline{w'\theta'_{\mathrm{v}}} u_*^2}, \quad (8)$$

ACPD
14, 7711–7737, 2014

where Δz is the distance between the sensors (8.2–2.23 m), $\overline{\theta_v}$, $\overline{w'\theta'_v}$ and u_* are measured at 2.23 m, and all the differences are calculated by using the measurements at this two sensors. We select these two sensors because this area with an evolution closer to the idea proposed by Bénard. Turbulent thermal diffusivity and turbulent viscosity could play a role in the initiation or the ceasing of convection. We define the transitional turbulent Rayleigh number (Ra_t) as the value of Ra_{turb} when the buoyancy flux ceases. Figure 8 shows the temporal evolution of buoyancy flux and Ra_{turb} from 17:00 to 20:00 UTC on 30 June and 1 July 2011. As can be observed, Ra_{turb} becomes negative later on 1 July 2011. For all the analyzed days, BF is negative several tens of minutes before Ra_{turb}. Table 1 shows this temporal difference and the value of Ra_t. As can be observed, this temporal difference is clearly related with DT being larger the days with a larger temporal difference between Ra_t and BF.

We assume that, on each day, Ra_t is in correspondence with the critical Rayleigh number (Ra_{cr}). It is important to notice that during early morning, on those days with large values of Ra_{cr} larger values of buoyancy flux are needed to onset convection. Additionally, during the evening transition on these days, convection stops quickly when the buoyancy flux ceases. By assuming $Ra_t \propto Ra_{cr}$, larger values of Ra_t have to be observed on these days. Figure 9 shows DT – t_* as a function of Ra_t for all the studied days. There is an exponentially decreasing relationship between both parameters. IOPs with larger Ra_t have a smaller difference between the convective and the delay time, meaning convection stops quickly. On the contrary, those days with low values of Ra_t, their convection slowed down smoothly increasing the delay time and consequently DT – t_*.

5 Conclusions

It has been shown that there is a clear failure of flux gradient theory during the evening transition period as a result of non-local processes. Analysis of the data obtained from a 10 m tower during the BLLAST campaign indicates that a delay time exists between

ACPD
14, 7711–7737, 2014

the time when the buoyancy flux ceases and the change in sign of the vertical gradient of the virtual potential temperature. This was the case for all IOPs.

For strong to moderate convective days, the delay time is relatively short (~ 30–40 min) and corresponds closely to the time scale associated with the last eddy movements. In other words, it is similar to the convective time scale. On the other hand, when midday convection is weaker, mechanical forces play a much larger role resulting in a larger friction velocity. In these cases, the delay time is larger due to the increase of horizontal turbulence. The data support an exponential relationship between the difference in the delay time and the convective time scale and the Monin–Obukhov parameter $-z/L$. If found to be generalizable, this relationship could be used to help forecast the delay time using midday measurements (for days where large scale forcings are changing slowly).

Finally, we defined a transitional turbulent Rayleigh number (Ra_t) associated with the buoyancy flux cease. We observe that higher values of Ra_t are related with a faster decay of the convection. Otherwise, turbulent viscosity and thermal diffusivity help to slow down the last eddy movement and increase the delay time when we observe low values of Ra_t.

Acknowledgements. The authors wish to thank Dr. Andrey Grachev for his thoughts and advice on the topic presented.

This project was performed under the Spanish MINECO projects CGL2009–08609, and CGL2012–37416–C04–03. The stage at the University of Utah was performed under the Spanish MINECO projects EEBB–I–12–05228. This work was partially supported by the United States Office of Naval Research, Award #N00014–11–1–0709.

The BLLAST field experiment was made possible thanks to the contribution of several institutions and supports: INSU-CNRS (Institut National des Sciences de l'Univers, Centre National de la Recherche Scientifique, LEFE–IDAO program), Météo-France, Observatoire Midi-Pirénées (University of Toulouse), EUFAR (EUropean Facility for Airborne Research) and COST ES0802 (European Cooperation in the field of Scientific and Technical). The field experiment would not have occurred without the contribution of all participating European and American research groups, which all have contributed in a significant amount. BLLAST field

ACPD
14, 7711–7737, 2014

experiment was hosted by the instrumented site of Centre de Recherches Atmosphériques, Lannemezan, France (Observatoire Midi-Pirénées, Laboratoire d'Aérologie). BLLAST data are managed by SEDOO, from Observatoire Midi-Pirénées.

References

Angevine, W. M.: Transitional, entraining, cloudy, and coastal boundary layers, Acta Geophys., 56, 2–20, 2007. 7714

Beare, R. J., Edwards, J. M., and Lapworth, A. J.: Simulation of the observed evening transition and nocturnal boundary layers: large-eddy modelling, Q. J. Roy. Meteor. Soc., 132, 61–80, 2006. 7713

Businger, J. A., Wyngaard, J. C., Izumi, Y., and Bradley, E. F.: Flux–profile relationships in the atmospheric surface layer, J. Atmos. Sci., 28, 181–189, 1971. 7733

Chapra, S. C. and Canale, R. P.: Numerical Methods for Engineers, 3rd Edn., McGraw-Hill Companies, Boston, 1998. 7717

Cole, G. S. and Fernando, H. J. S.: Some aspects of the decay of convective turbulence, Fluid Dyn. Res., 23, 161–176, 1998. 7714, 7715

Deardorff, J.: Numerical investigation of neutral and unstable planetary boundary layers, J. Atmos. Sci., 7, 91–115, 1972. 7713, 7721

Edwards, J. M., Beare, R. J., and Lapworth, A. J.: Simulation of the observed evening transition and nocturnal boundary layers: single-column modelling, Q. J. Roy. Meteor. Soc., 132, 61–80, 2006. 7714

Fedorovich, E., Nieuwstadt, F. T. M., and Kaiser, R.: Numerical and laboratory study of horizontally evolving convective boundary layer. Part II: Effects of elevated wind shear and surface roughness, J. Atmos. Sci., 58, 546–560, 2001. 7712

Franchitto, S. H. and Rao, V. B.: The correlation between temperature gradient and eddy heat flux in the Northern and Southern Hemispheres, J. Meteorol. Soc. Jpn., 81, 163–168, 2003. 7713

Ghan, S. J.: Modelling the synoptic scale relationship between eddy heat flux and the meridional temperature gradient, M.S. thesis, Dept. of Meteorology and Physical Oceanography, Massachusetts Institute of Technology, 65 pp., 1981. 7713

ACPD
14, 7711–7737, 2014

Grimsdell, A. W. and Angevine, W. M.: Observations of the afternoon transition of the convective boundary layer, J. Appl. Meteorol., 41, 3–11, 2002. 7714
Haeffelin, M., Angelini, F., Morille, Y., Martucci, G., Frey, S., Gobbi, G. P., Lolli, S., O'Dowd, C. D., Sauvage, L., Xueref-Rémy, I., Wastine, B., and Feist, D. G.: Evaluation of mixing-height retrievals from automatic profiling lidars and ceilometers in view of future integrated networks in Europe, Bound.-Lay. Meteorol., 143, 49–75, 2012. 7721
Holtslag, A. A. M. and Moeng, C.: Eddy diffusivity and countergradient transport in the convective atmospheric boundary layer, J. Atmos. Sci., 48, 1690–1698, 1991. 7713
Kundu, P. J. and Cohen, I. M.: Fluid Mechanics, Academic Press, Waltham (MA), USA, 904 pp., 2010. 7715
Lothon, M. and Lenschow, D.: Studying the afternoon transition of the planetary boundary layer, Eos T. Am. Geophys. Un., 91, 253–260, 2010. 7713
Lothon, M., Couvreux, F., Durand, P., Hartogensis, O., Legain, D., Lohou, F., Pardyjak, E. R., Pino, D., Reuder, J., Vilà-Guerau de Arellano, J., Alexander, D., Augustin, P., Bargain, E., Barrié, J., Bazile, E., Bezombes, Y., Blay, E., van de Boer, A., Boichard, J. L., de Coster, O., Cuxart, J., Dabas, A., Darbieu, C., Deboudt, K., Delbarre, H., Derrien, S., Faloona, I., Flamant, P., Fourmentin, M., Garai, A., Gibert, F., Gioli, B., Graf, A., Groebner, J., Guichard, F., Jonassen, A., von Kroonenbeerg,M, Lenschow, D., Martin, S., Martinez, D., Mastrorillo, L., Moene, A., Molinos, F., Moulin, E., Pietersen, H., Piguet, B., Pique, E., Román-Gascón, C., Saï d, F., Sastre, M., Seity, Y., Steeneveld, G. J., Toscano, P., Traullé, O., Tzanos, D., Yagüe, C., Wacker, S., Wildmann, N., and Zaldei, A.: The Boundary Layer Late Afternoon and Sunset Turbulence 2011 field experiment, in: 20th Symposium on Boundary Layers and Turbulence, 9–13 July 2012, Westin Copley Place, Boston, MA, Paper 14B.1, 2012. 7713, 7721
Mahrt, L.: Nocturnal boundary-layer regimes, Bound.-Lay. Meteorol., 88, 255–278, 1998. 7713
Moeng, C.-H. and Sullivan, P. P.: A comparison of shear- and buoyancy-driven planetary boundary layer flows, J. Atmos. Sci., 51, 999–1022, 1994. 7712
Nadeau, D. F., Pardyjak, E. R., Higgins, C. W., Fernando, H. J. S., and Parlange, M. B.: A simple model for the afternoon and early evening decay of convective turbulence over different land surfaces, Bound.-Lay. Meteorol., 141, 301–324, 2011. 7713, 7714
Nieuwstadt, F. T. M.: The turbulent structure of the stable, nocturnal boundary layer, J. Atmos. Sci., 41, 2202–2216, 1984. 7713

ACPD
14, 7711–7737, 2014

Nieuwstadt, F. T. M. and Brost, R. A.: The decay of convective turbulence, J. Atmos. Sci., 43, 532–546, 1986. 7721

Pino, D., Jonker, H. J. J., Vilà-Guerau de Arellano, J., and Dosio, A.: Role of shear and the inversion strength during sunset turbulence over land: characteristic length scales, Bound.-Lay. Meteorol., 121, 537–556, 2006. 7714

Pino, D., Vilà-Guerau de Arellano, J., and Duynkerke, P. G.: The contribution of shear to the evolution of a convective boundary layer, J. Atmos. Sci., 60, 1913–1926, 2003. 7712

Sahlée, E., Smedman, A., Rutgersson, A., and Högström, U.: Influence of a new turbulence regime on the global air–sea heat fluxes, J. Climate, 121, 5925–5941, 2007. 7720

Smedman, A., Högström, U., Hunt, J. C. R., and Sahlée, E.: Heat/mass transfer in the slightly unstable atmospheric surface layer, Q. J. Roy. Meteor. Soc., 133, 37–51, 2007. 7720

Sorbjan, Z.: Effects caused by varying the strength of the capping inversion based on a large eddy simulation model of the shear-free convective boundary layer, J. Atmos. Sci., 53, 2015–2024, 1996. 7712

Sorbjan, Z.: Decay of convective turbulence revisited, Bound.-Lay. Meteorol., 82, 503–517, 1997. 7714, 7719

Stull, R. B.: An Introduction to Boundary Layer Meteorology, D. Reidel Publ. Comp., Dordrecht, the Netherlands, 670 pp., 1988. 7712, 7719

Sullivan, P. P., Moeng, C.-H., Stevens, B., Lenschow, D. H., and Mayor, S. D.: Structure of the entrainment zone capping the convective atmospheric boundary layer, J. Atmos. Sci., 55, 3042–3064, 1998. 7712

Van Dijk, A., Moene, A. F., and De Bruin, H. A. R.: The principles of surface flux physics: theory, practice and description of the ECPACK library, Internal Report 2004/1, Meteorology and Air Quality Group, Wageningen University, Wageningen, the Netherlands, 99 pp., 2004. 7716

van Driel, R. and Jonker, H. J. J.: Convective boundary layers driven by nonstationary surface heat fluxes, J. Atmos. Sci., 68, 727–738, 2011. 7719

ACPD
14, 7711–7737, 2014

Table 1. Based on the observations taken at BLLAST campaign, IOP day, maximum sensible heat flux, length of the day, days from last rainfall, delay time, convective time, convective intensity, transitional turbulent Rayleigh number and temporal difference between the time when *Ra* changes sign and buoyancy flux does it.

Day (IOP)	SH_{max} ($W m^{-2}$)	Diurnal cycle (h)	Sunset (UTC)	Days from last rainfall	DT (min)	t_* (min)	$-z/L$	Convective definition	Ra_t	Ra_t – BF (min)
24 Jun (IOP4)	0.18	13.3	19:42	1	38	36	0.297	Convective	9.89	49
25 Jun (IOP5)	0.158	12.8	19:42	2	48	26.37	0.102	Weak	1.097	90
27 Jun (IOP7)	0.1	10.25	19:42	4	72	42	0.1205	Weak	3.62	95
30 Jun (IOP8)	0.11	12.16	19:42	1	30	27	0.289	Convective	10.32	34
1 Jul (IOP9)	0.138	12.8	19:41	2	40	33	0.22	Moderate	5.01	55
2 Jul (IOP10)	0.14	11.3	19:41	3	42	55.8	0.24	Moderate	4.5	53

ACPD
14, 7711–7737, 2014

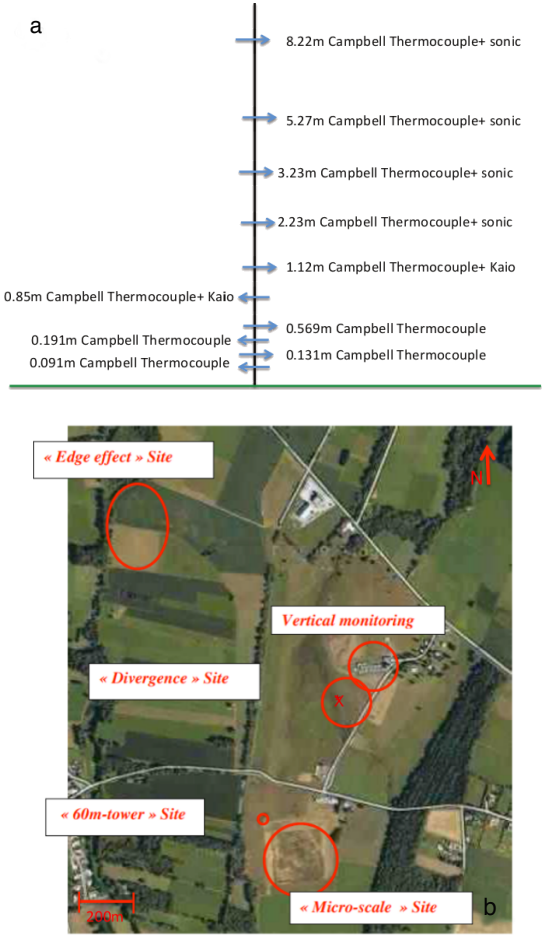

Fig. 1. (a) Sketch of the distribution of sensors that were deployed on the 10 m mast during BLLAST and **(b)** an aerial view of the site (the red X indicates the location of the 10 m tower).

ACPD
14, 7711–7737, 2014

Countergradient heat flux observations during the evening transition period

E. Blay-Carreras et al.

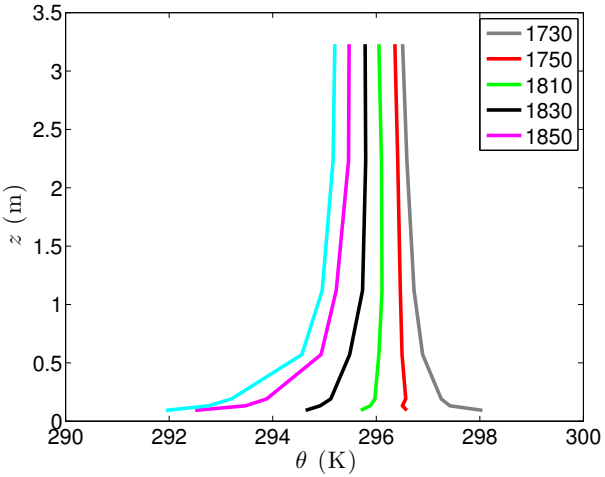

Fig. 2. Observed 5 min averaged vertical profile of potential temperature during the evening transition on 1 July 2011.

ACPD
14, 7711–7737, 2014

Countergradient heat flux observations during the evening transition period

E. Blay-Carreras et al.

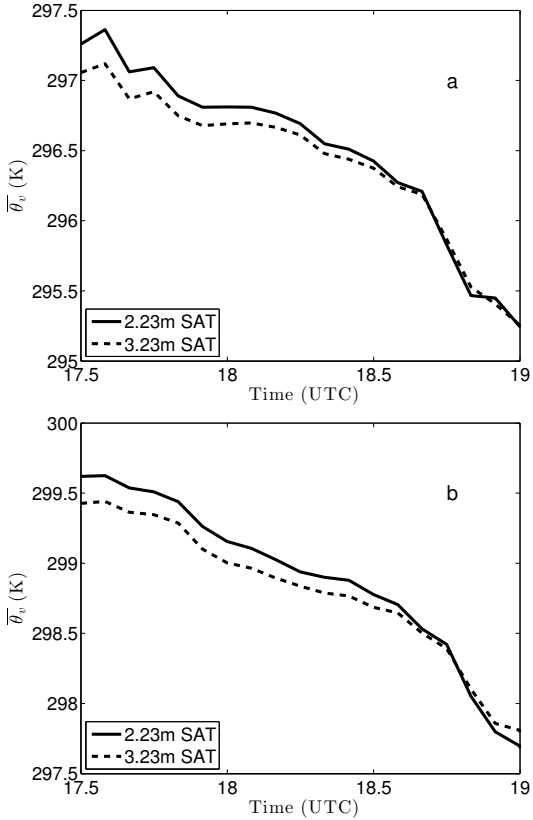

Fig. 3. Observed temporal evolution of the virtual potential temperature at 2.23 m (solid line) and 3.23 m (dashed line) during the evening transition on **(a)** 30 June and **(b)** 1 July 2011.

ACPD
14, 7711–7737, 2014

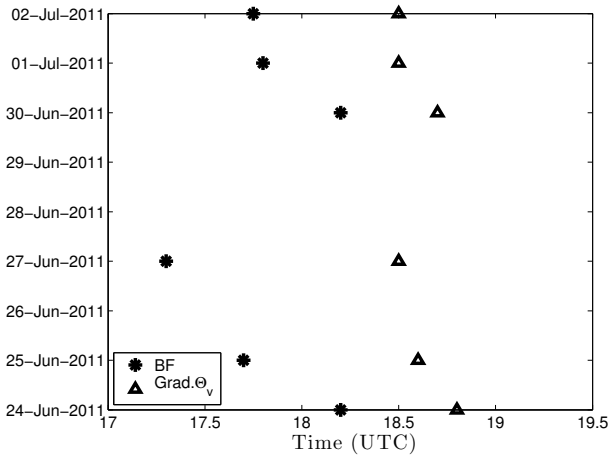

Fig. 4. For each IOP, instant when buoyancy flux (asterisks) and virtual potential temperature gradient (triangles) change sign.

ACPD
14, 7711–7737, 2014

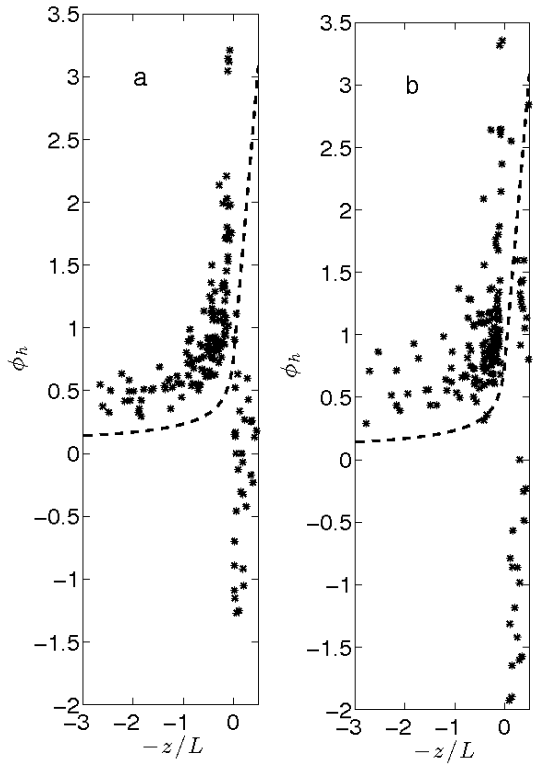

Fig. 5. Dimensionless temperature gradient (ϕ_h) as a function of $-z/L$ at 2.23 m on **(a)** 30 June and **(b)** 1 July 2011. Dashed line is the approximation of Businger et al. (1971).

ACPD
14, 7711–7737, 2014

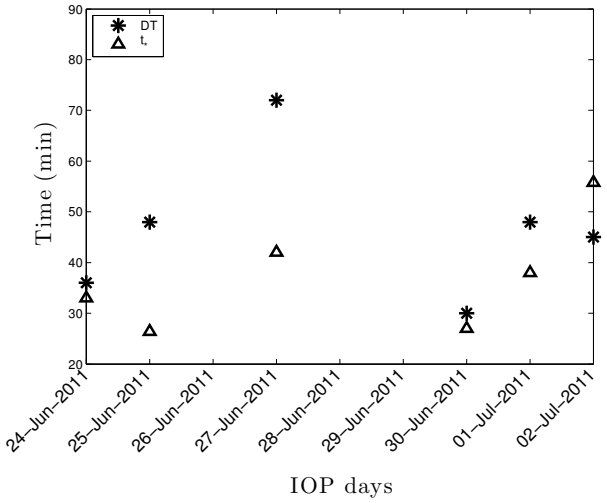

Fig. 6. For each IOP, delay (asterisks) and convective (triangles) times.

ACPD
14, 7711–7737, 2014


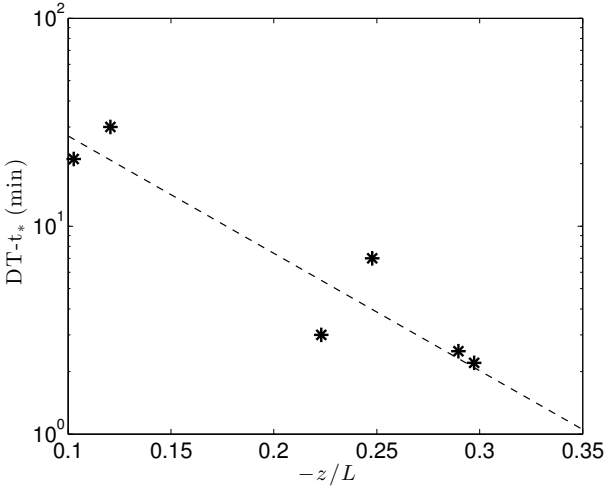

Fig. 7. For all the IOPs, difference between the delay and convective times as a function of $-z/L$.

ACPD
14, 7711–7737, 2014

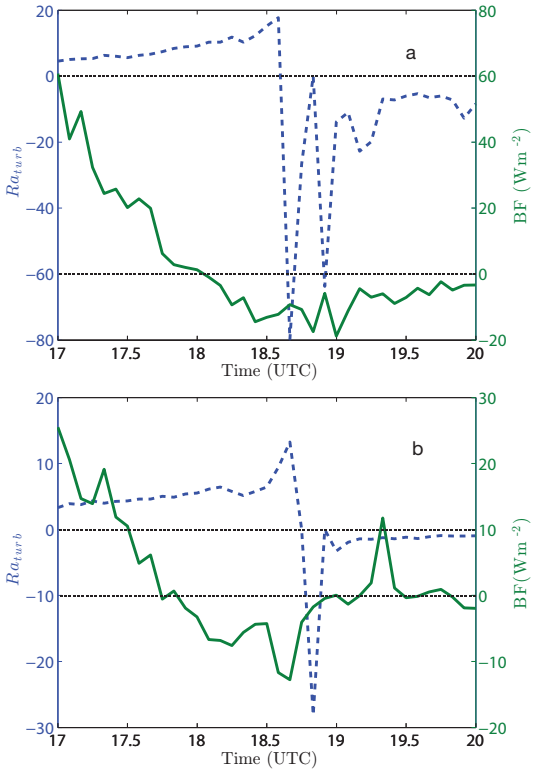

Fig. 8. Temporal evolution of buoyancy flux at 2.23 m (green) and Ra_{turb} (blue) during the evening on **(a)** 30 June and **(b)** 1 July 2011.

ACPD
14, 7711–7737, 2014

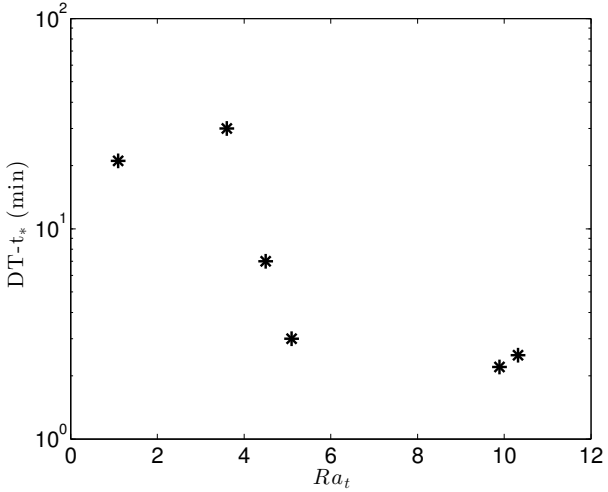

Fig. 9. For all the IOPs, difference between the delay and convective times as a function of transitional turbulent Rayleigh number (Ra_t).

ACPD
14, 7711–7737, 2014